

# **Real-Time Continuous Surface Modeling of Massive Geospatial Point Clouds with User-Selectable Entities**

Student: Stephen Ranger

Advisor: Professor Reynold Bailey

RIT Department of Computer Science

Thesis

## **Abstract**

Massive point cloud data sets are currently being created and studied in academia, the private sector, and the military. Many previous attempts at rendering point clouds have allowed the user to visualize the data in a three-dimensional way but did not allow them to interact with the data and would require all data to be in memory at runtime. Recently, a few systems have cropped up that deal with real-time rendering of massive point clouds with on-the-fly level of detail modification that handles out-of-core processing but these systems have their own limitations. With the size and scale of massive point cloud data coming from LiDAR (Light Detection and Ranging) systems, being able to visualize the data as well as interact and transform the data is needed.

Previous work in out-of-core rendering [3] [4] [5] showed that using Octrees and kd-trees can increase the availability of data as well as allow a user to visualize the information in a much more useful manner. However, viewing the data isn't enough; applying work in context-aware selection [2] and surface creation [1] the visualization system would greatly benefit in usability and functionality.

# Table of Contents

Chapter 1: Background.....	4
Quadtrees.....	4
Octrees.....	5
KD-Trees.....	5
Chapter 2: Methodology.....	8
Chapter 3: Design.....	9
Partitioning Application.....	9
Visualization Tool.....	12
Rendering Component.....	12
Selection Algorithm.....	14
Chapter 4: Evaluation.....	16
Chapter 5: Evaluation Outcomes.....	16
Octree and Icosatree Building Statistics.....	16
Point Selection and Triangulation.....	18
Octree vs Icosatree Cell Size and Rendering Statistics.....	20
Chapter 6: Deliverables.....	24
References.....	25

# Illustration Index

Illustration 1: Quadtree Structure [10].....	4
Illustration 2: Octree Structure and Flattened Tree [11].....	5
Illustration 3: Two-Dimensional KD-Tree Structure [12].....	6
Illustration 4: KD-Tree Partitioning Example [13].....	7
Illustration 5: Icosatree Wireframe.....	10
Illustration 6: Icosatree Cells.....	11
Illustration 7: Tree File Structure.....	11
Illustration 8: Visualization Application with Small Point Cloud.....	13
Illustration 9: Selection Lasso.....	15
Illustration 10: Selected Points.....	15
Illustration 11: Point triangulation.....	15
Illustration 12: Triangular Coordinates.....	17
Illustration 13: Point Selection with Lasso.....	19
Illustration 14: Selection Triangulation.....	19
Illustration 15: Selection Triangulation with Obstruction Pruning.....	20
Illustration 16: Selection Triangulation Closeup.....	20
Illustration 17: Rendering Statistics Sample Image (depth = 10.0).....	22
Illustration 18: Rendering Statistics Sample Image (depth = 3.0).....	23
Illustration 19: Rendering Statistics Sample Image (depth = 6.0).....	24

## **Index of Tables**

Octree Building Statistics.....	17
Icosatree Building Statistics.....	18
Octree Cell Statistics.....	20
Icosatree Cell Statistics.....	21
Rendering Statistics (depth = 10.0).....	21
Rendering Statistics (screen ratio = 3.0).....	22
Rendering Statistics (screen ratio = 6.0).....	23

# Chapter 1: Background

The basis for this continued work stems from multi-dimensional data structures and how they are leveraged in a geospatial environment. These data structures, the quadtree, Octree, and kd-tree, are used to partition a (usually) cartesian coordinate system into a tree structure.

## Quadtrees

The Quadtree separates a two-dimensional coordinate system into a tree structure where each node in the tree is split along the center of both axes within its axis-aligned bounding volume creating four child nodes. This allows for much more efficient searching than a simple data structure like an array or list would. Below, Illustration 1 shows a set of points in a two-dimensional cartesian coordinate system stored in a quadtree where each node that has only a single point remaining does not split again; thus saving computational time and storage space. The Quadtree structure is used in geospatial visualizations as it aligns to the longitude and latitude coordinate system, however, the disconnect along the 180-degree meridian and the difficult-to-handle north and south border meeting at a single point cause more issues.

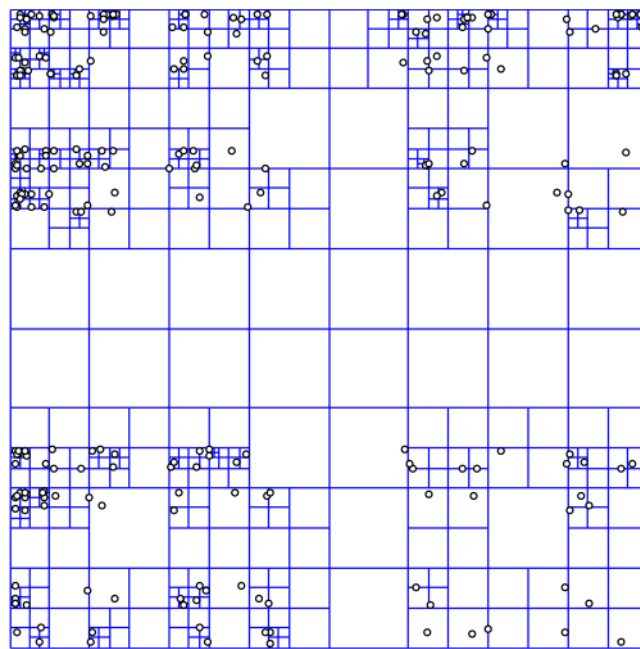


Illustration 1: Quadtree Structure [10]

## Octrees

The Octree structure is identical to the quadtree structure except that it is applied to a three-dimensional coordinate system. Each node is split into potentially eight child nodes but it still uses a uniform split location by bisecting the span along each axis of its axis-aligned bounding volume. The Octree is used quite often in Computer Graphics as it fits well to an XYZ cartesian coordinate system and allows culling, bounds intersection, and mouse picking for many objects quickly and efficiently. However, in a geospatial visualization, this structure does not align well to an elliptical surface such as the Earth. Below, Illustration 2 is an image of an Octree in 3D as well as the flattened version of the tree.

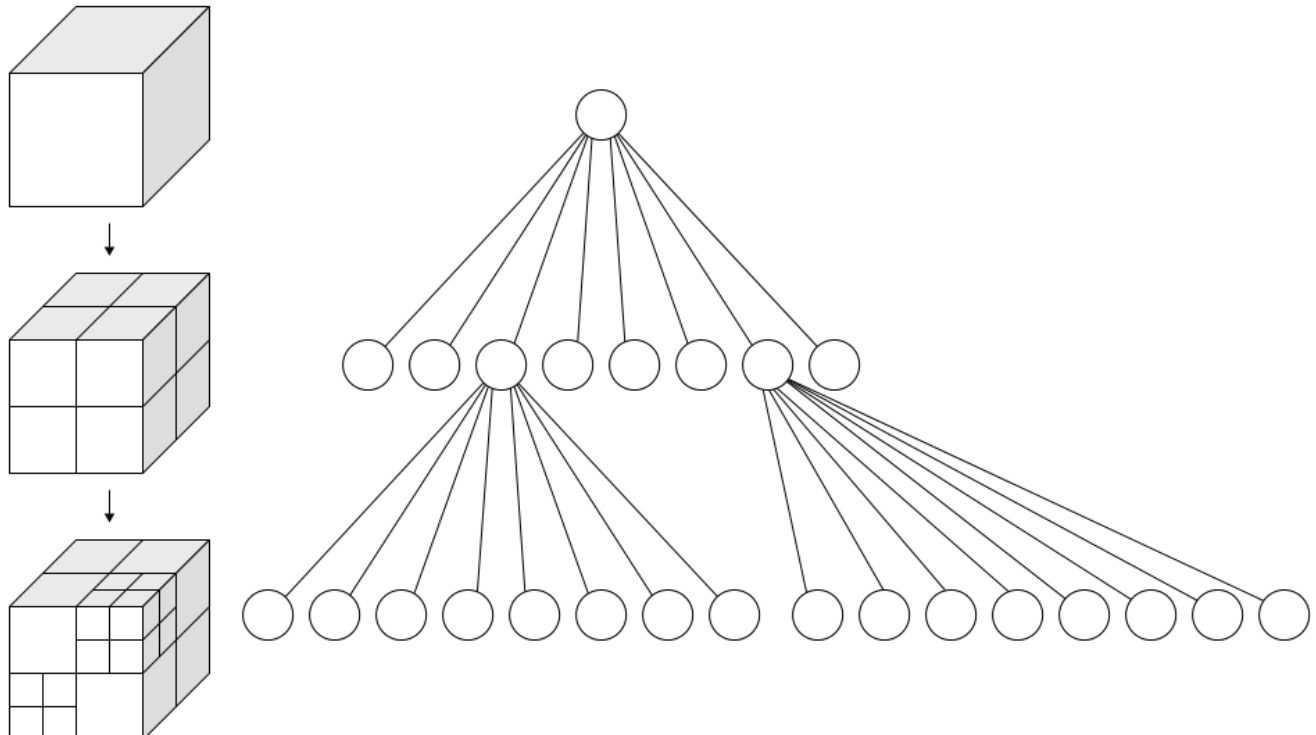
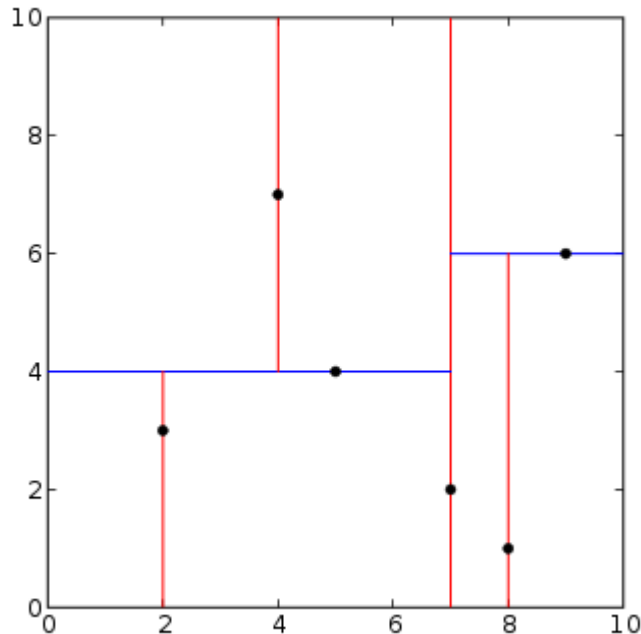


Illustration 2: Octree Structure and Flattened Tree [11]

## KD-Trees

The KD-Tree is a specialized binary tree that allows for more control over how the tree is structured as well as lending itself to being more uniform and balanced than previously mentioned tree data

structures. The KD-Tree, at each level, chooses a single axis to split along. The axis chosen is defined by a set of criteria such as which axis has the longest span between its min and max values. Then, the split location is also defined by a set of criteria such as splitting each side into containing a uniform number of points. The actual split location, unlike the quadtree and Octree, is a single point that acts as the node in the tree at that depth. This continues until each node has a single point or until some threshold is reached based on tree depth or point count. The KD-Tree is a binary tree but can be used with any dimensionality which allows it to be applied to a two-dimensional longitude-latitude coordinate system as with the quadtree and an XYZ cartesian coordinate system like the Octree. It has many of the same drawbacks when it comes to applying it to a geospatial coordinate system. However, one upside is that it can be built in such a way that each node has a relatively uniform number of points which can increase storage efficiency and render times by allowing us to store nodes in chunks without wasting padded space but with the drawback that level-of-detail algorithms make the scene seem non-uniform as each node is rendered and the node dimensions are not consistent. Below, Illustration 3 shows a two-dimensional KD-Tree partitioning algorithm with red and blue lines as alternating split locations. Illustration 4 shows the flattened tree structure for part of the previous illustration and which axis was used at each level.



*Illustration 3: Two-Dimensional KD-Tree Structure [12]*

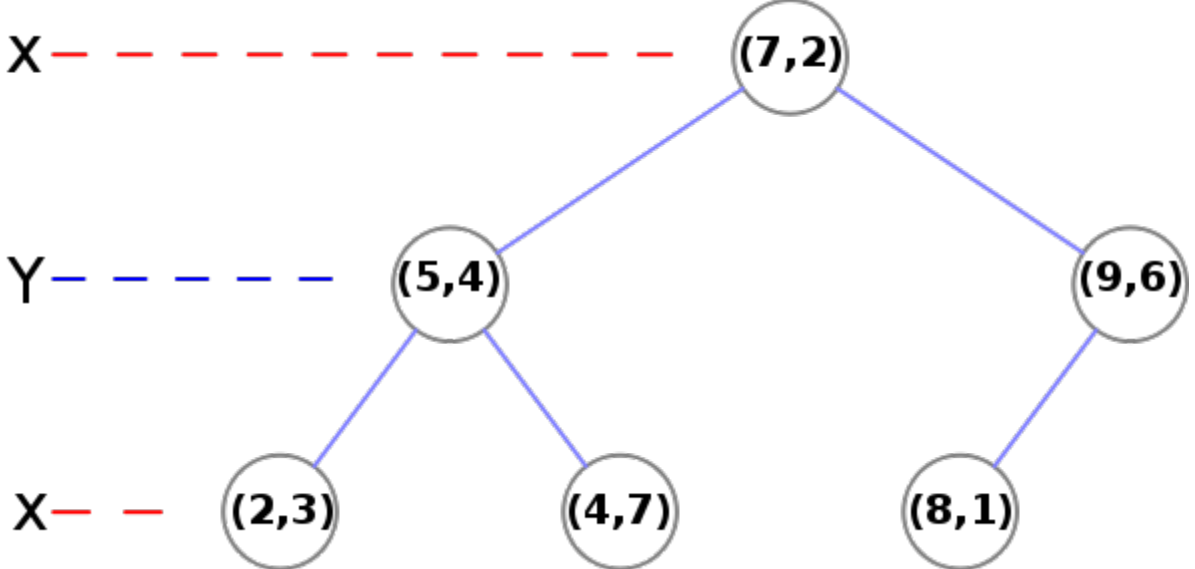


*Illustration 4: KD-Tree Partitioning Example [13]*

Previously, quadtree, Octree [3] and kd-tree partitioning systems have been applied to a Cartesian system in order to add on-demand searching for view-dependent slices of data. However, once the data set is converted into a geospatial positioning system, either the Cartesian coordinates are now not surface aligned, or issues arise along the partitioning system boundaries where values are not continuous (such as with latitude  $90 \neq -90$  but longitude  $180 = -180$ ). Using a Cartesian projection from geospatial coordinates solves this issue but adds complexity when deciding what to render as it is no longer surface aligned. I will look into applying a surface-aligned data structure to a global data set such as a tetrahedral mesh. By using this structure to search for nodes within my view frustum I will be able to render progressively deeper nodes as the visualization's viewpoint moves closer or further away from the target and as the level of detail increases and pull these nodes from an on-demand point server.

Also, in recent work, real-time rendering of depth culling and surface representation [1] has been used to hide unseen data points as well as to fill surface information in on a massive unstructured point cloud. I propose to use this information and apply it to a sparse context-aware selection algorithm [2] in order to adapt it to a more uniformly dense data set. I believe that this on-the-fly surface creation can be used to augment the context-aware selection algorithm in order to give it another avenue for object separation within a uniformly-dense data set.

## Chapter 2: Methodology

Previous work in the field of massive point cloud creation and processing has moved toward data systems [6] such as OpenTopography.org as well as research in leveraging Octree and kd-tree data structures for taking massive point cloud data and partitioning it into manageable pieces for the visualization system. Separate work in selection and surface generation have increased the user interaction and utility of these types of datasets. However, tree structures in cartesian or geodetic coordinate systems each have their own drawbacks and limiting the user to visualization alone gives them a powerful tool with nothing to use it for.

The first hurdle is to look at the state of data partitioning and access. Currently, Octrees and kd-trees work in a cartesian coordinate system. With point cloud data that is relatively limited in size and scope, using an arbitrary coordinate system can work well. Moving towards larger data sets and rendering them on a geospatial projected surface and now your data no longer follows an axis-aligned format. This causes more issues with rendering such as data structures that clip the projected surface and do not fill the partitioned sections well. The first goal of this research is to modify the data structure used to store the massive point cloud data from an Octree/kd-tree structure where the XYZ cartesian grid doesn't align well with a geospatial projected surface (WGS84) into an icosahedral grid using previous work in spherical self organizing grids [7] and traversal of triangle mesh elements [8] [9]. Allowing the data to be split into surface aligned data structures should look more pleasing to the end user as the level of detail is modified on-the-fly compared to an Octree/kd-tree structure without the need of overrawing or forcing the user to wait until all data is available before rendering.

The second hurdle is to add functionality to the system instead of just being a visualization system. Previous work in the area consisted of interacting with unstructured point clouds [2] by allowing the user the ability to select more-dense regions of data using a screen-space masking system. However, this implementation is limited by requiring the data be unstructured, or containing a very heterogeneous density throughout. Unfortunately, LiDAR data is rarely sparse; it is rarely pruned or processed at all

before being accessed by researchers. In another area, on-the-fly surface creation has been applied to point cloud data in order to show physical structures [1] in the input data; this shows off actual objects in the virtual world without having extensive up-front processing of the data. This surface modeling can be leveraged against the context-aware selection algorithm in a uniformly dense point cloud to allow the user to select via screen-space masking controls objects in the LiDAR point cloud data. From this, the point data can be displayed separately for further study or exported for use in other applications.

In order to evaluate these assumptions, the author has developed a number of utility applications as well as a simple visualization designed to load a point cloud and allow the end user to modify the rendering settings, use a screen-selection lasso for object selection, and the display and export of selected points and resulting triangulation. The utilities developed consist of command line applications that will access a binary file of point data along with a csv of point attributes. The application then partitions and exports the data as either an Octree or Icosatree for use with the visualization application. A command line application was also created to partition the binary input file into smaller portions for ease of use and testing. Lastly, the visualization system was developed using a number of previously developed graphics and computation libraries developed by the author for previous work as well as a number of third party, open source, libraries.

## Chapter 3: Design

The system designed for this research contains four major pieces: A Partitioning application, A Visualization tool, The Rendering Component, and the Selection Algorithm. Below is a detailed explanation of their implementation and theory.

### Partitioning Application

The partitioning application is a standalone command line application that reads from a number of binary point data files. It creates the different partitioning systems needed to evaluate the algorithm

implementations and stores them in a custom binary format for ease of access at runtime. The files have been designed so that they can be accessed via the local file system or through a web server.

The data structure has been partitioned such that each level in the tree structure, for both the Octree and Icosatree, contains points which are left in each node. The nodes are split into a subcell grid structure so all nodes at a specific depth are uniformly dense in order for the level of detail algorithm to only have to deal with screen area and not point densities within the visualization tool when determining how deep to traverse. The data also contains information defining the number of points in the node, the number of child nodes, and the layout of the binary data (at the root, only).

The structure of the Octree and Icosatree file systems are fairly straightforward. Each is defined by a file tree originating at a given root directory. Then in each directory, including the root, a point data file exists along with an ASCII text file containing a list of the existing child nodes at that location. The root directory also contains a CSV file defining the binary layout of the point data which contains information about attributes: name, offset, data type, size in bytes, min, max, mean, and variance.

The Octree and Icosatree structures are identical except for the fact that each Octree cell contains, at most, eight child cells. The Icosatree root node can contain up to twenty child cells and each cell after that can contain at most eight. The Octree structure is split along the XYZ axes as in Illustration 2. However, the Icosatree is split into twenty triangular prism cells at the root as in Illustration 5. Below that, each cell is split into eight additional triangular prisms as seen in Illustration 6.

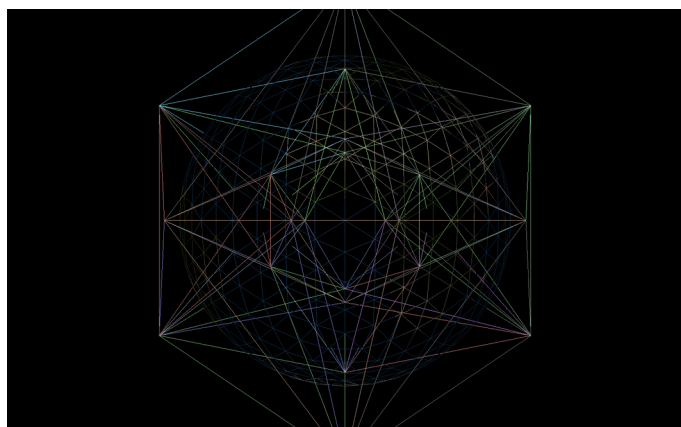


*Illustration 5: Icosatree Wireframe*

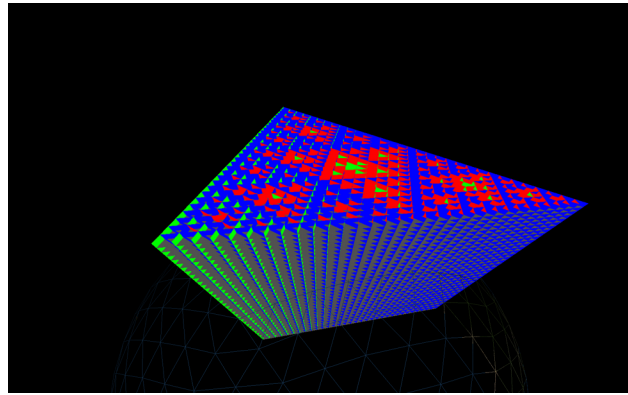


*Illustration 6: Icosatree Cells*

Each cell is also split into subcells; this allows the tree creation to guarantee uniform density of point data at any specific level of the tree which greatly simplifies level of detail calculations in the renderer. As the tree structure is built, a point is inserted into the root node. The subcell is computed and if no point was previously added there, the current point is stored. If a point was previously stored at that subcell index, the point closest to its centroid is left there and the remaining point is sent to one of the cells' child cells. This continues until all points have been added to the tree. Once that is complete, the command line tool writes the tree structure as a set of directories and binary or ASCII files. A subset of this file structure can be seen in Illustration 7. The dat file contains the binary point data and the text file contains the child cell index values which contain point data of their own. These child cells also have a sub-directory within that nodes' directory which continues to the leaves of the tree.

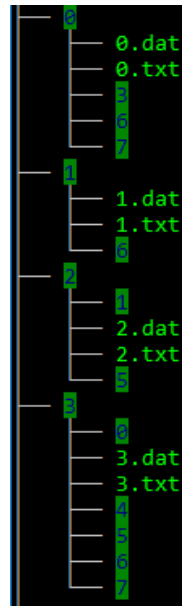


*Illustration 7: Tree File Structure*

## Visualization Tool

The visualization tool consists of a Java/OpenGL rendering system based off the Java OpenGL Library (JOGL) and a rendering toolkit the author has developed. Simple geospatial navigation and terrestrial terrain have been added as they aid the user when interacting and visualizing this form of data. The visualization renders a simple WGS84 projected globe, a spherical orbit navigator, the point cloud renderer which supports the different data structures implemented by the partitioning application, and the selection algorithm used by the user which allows them to select objects, as the points that comprise them, from the scene using a screen-space lasso tool.

The visualization tool renders each item in the scene as its own scene element. The camera navigation is based on a geospatial anchor point and an azimuth/elevation/distance offset from the anchor. A local origin will offset the scene component's local coordinate system for floating point precision reasons and each scene element will update its own position based on this local origin.

## Rendering Component

The rendering component initially reads the root node and attributes layout information from the dataset (locally or over the web). It then uses the bounding volume of the node to determine if it should be rendered or not and if its children should be queried. It then uses a screen-space level of detail algorithm to determine how deep to traverse; this depth will be tunable based user preference.

The Octree and Icosatree are both supported by the rendering component as their data structures are identical aside from the number of children their root nodes may contain. The class TreeRenderable is given a path (either local or http) to the root of the tree data and a ConnectionType. Each frame, it does a frustum culling pass to determine which tree cells should be included in the rendering step. Then, for each cell it checks its on-screen area. This area calculation is used to compare against two different thresholds; the first is if this node should render any points it may contain ( $50 \times 50$  pixels) and the second is if its children should be checked ( $200 \times 200$  pixels). The nodes are split into two sets; those

that are complete and those that are pending. The complete nodes have their point data already retrieved while the pending nodes have been created but are still waiting for their point data to be accessed by the connection thread. Next, a small portion of the frame time is given over for uploading data to the graphics card; this is limited in order to keep the visualization at an interactive frame rate. The vertex buffer implementation is actually a number of buffer pools, each of which contain a number of vertex buffer objects and the pool is able to allocate and delete these objects as needed. The tree structure contains the maximum number of points necessary for any node in the tree; this is the starting segment size for the buffer pools. The first pool is defined by a number of segments (100 by default) which can each hold this maximum number of points per buffer object (byte size equal to the attribute-stride \* max points \* segments per buffer). Then, another pool is made by dividing the segment size by two and continuing this until the smallest buffer object is sliced into segments less than 100 points long. This allows a number of different sized cells to be inserted into a buffer that, at least, fills half of its total capacity but also allows the rendering system to intelligently add, remove, and update cells in the tree without having to pack or rearrange data on the graphics card every frame. Below, in Illustration 8, is a screenshot of Morro Bay in California; this is a subset of the San Simeon, CA point cloud dataset and, in total, contains 13,725,592 points. At the current zoom distance and level of detail the rendering component is only required to render around three million points.

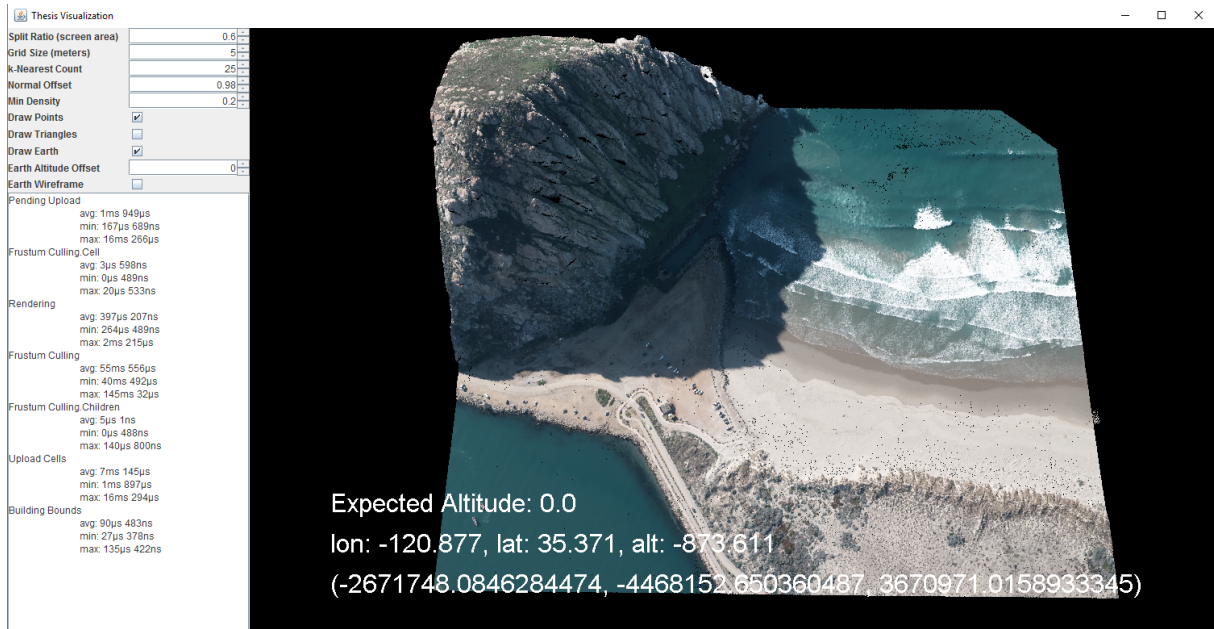


Illustration 8: Visualization Application with Small Point Cloud

## Selection Algorithm

The selection algorithm attempts to apply portions of two separate point cloud selection algorithms to the same set of data. The Screen-Space Operator Algorithm [1] is used to define surfaces inside the point cloud; this is useful for visualizing the walls of buildings and such. However, the algorithm itself doesn't handle selection of objects. The CAST algorithm [2] allows selection of more dense portions of a point cloud via two-dimensional mouse selection but it requires a dense cloud of points to handle selection. I have attempted to apply the screen-space lasso and point density techniques from the CAST algorithm and apply the surface creation and triangulation algorithm to the resulting selection in order to give a user more utility when analyzing a point cloud dataset.

The first step of the algorithm is for the user to define the search area. This is done in the visualization by holding the control key and holding the left mouse button while defining the lasso area. The shape is automatically connected to the initial selection point as the user outlines the lasso shape but the final polygon will be automatically closed the first time the lasso crosses itself in order to create a closed loop.

Then, a simple volume frustum is created from the camera into the scene along the screen-space lasso polygon. The tree is searched and any points that are contained within the lasso are returned. Next, for each point, the k-nearest neighboring points are queried and a covariance matrix is computed. If the normal of the best-fit plane of the entire selection is parallel (or within a user-defined threshold) the point is dropped from the selection. Finally, any points whose most distant neighbor is further than twice the user-defined grid size is also removed. This removes any points that are parallel to the ground as well as any points that are in small groups and aren't useful (less than the k-nearest limit).

In order to handle triangulation, the Screen-Space Operator Algorithm is used to determine which points in the selection are unobstructed. This is done by projecting a ray from each point towards the camera and, if any other point is within a specified angular distance and closer to the camera than the tested point, it is removed. These points are then converted into a two-dimensional plane and a

Delaunay triangulation algorithm is used to triangulate them. A map of the 2D projected point to the original 3D point is used to convert this triangulation back into a useful triangle mesh. The lasso (Illustration 9), point selection (Illustration 10), and triangle mesh (Illustration 11) can be seen below.



Illustration 9: Selection Lasso



Illustration 10: Selected Points



Illustration 11: Point triangulation

## Chapter 4: Evaluation

In order to evaluate my designs, the visualization system has the ability to collect, analyze, and export runtime and rendering metrics for the application and the tree building application exports a number of timing metrics based on elapsed time for building the tree, exporting to disk, the maximum and average points per tree cell, and the maximum cell depth.

## Chapter 5: Evaluation Outcomes

Tree building was done on an HP Z820 Workstation with an Intel Xeon E5-2650, 256GiB RAM, and a 1TB and 2TB Samsung 850 Pro SSD's. The MapDB library was used for point storage by tree cell and index and in place of in-memory storage, a filesystem map was used and stored on the 1TB SSD. The input point data was stored on the 2TB SSD and the output tree structure was written there as well; this was to make sure the MapDB file was not interfering with reading or writing the point data.

The data set used was a subset of the Morro Bay area from the San Simeon, CA dataset [15]. The area used falls within (-120.88, 35.36) and (-120.84, 35.40). It contains a total of 163,251,931 points.

### Octree and Icosatree Building Statistics

The Octree building statistics were run with a few different subcell sizes. A Table of subcell size, elapsed times, max and average points per cell, max tree depth, directory and file count, and total file size can be found in Table 1 and Table 2. With the Icosatree, attempts were made initially using barycentric coordinates as the basis of the indexing system but because barycentric coordinates are a weighted average position within the triangle and not an absolute weight for each vertex the system didn't work as intended. Later, a naive axis-aligned index was used in the same fashion as the octree subcell index but most of the index range went unused. Finally, a triangular coordinate system was developed that computes a position based on the projected position along two of the triangular edges. The triangular coordinate system computes a subcell index by splitting one edge into n-sections. Then, a second edge is also split into n-sections, however, it is numbered in both directions; columns of subcells oriented left-to-right and right-to-left. Then, each subcell is numbered with a triple coordinate

index. A point is inserted into a subcell along the top face of the triangular prism volume and then offset by depth into the volume by splitting the depth by m-sections. A diagram of the triangular coordinates can be seen in Illustration 12.

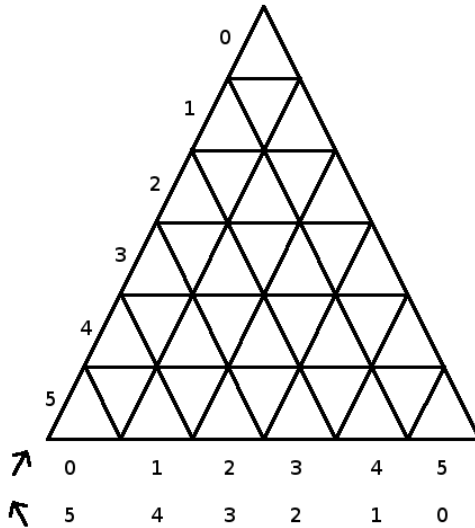


*Illustration 12: Triangular Coordinates*

SubCell Size	Tree Creation Time	Cells Created	Filesystem Export Time	Max Points Per Cell	Average Points Per Cell	Max Tree Depth	Directory Count	File Count	Total File Size
50x50x50	5h 8m	1,093,494	20m 48s	15548	150	32	1,093,494	2,186,989	11 GiB, 124 MiB
100x100x100	4h 42m	389,771	15m 55s	44223	419	31	389,771	779,543	11 GiB, 109 MiB

*Table 1: Octree Building Statistics*

SubCell Size	Tree Creation Time	Cells Created	Filesystem Export Time	Max Points Per Cell	Average Points Per Cell	Max Tree Depth	Directory Count	File Count	Total File Size
100x100x100	5h 25m	725,672	26m 41s	17123	225	32	725,672	1,451,345	11 GiB, 115 MiB
100x20	7h 18m	653,475	32m 38s	10233	250	31	653,475	1,306,951	11 GiB, 114 MiB
100x100	6h 27m	583,163	25m 43s	14569	280	31	583,163	1,166,327	11 GiB, 112 MiB
150x100	6h 14m	340,758	23m 54s	22618	480	30	340,758	681,517	11 GiB, 107 MiB
200x100	5h 49m	235,156	20m 4s	38081	695	29	235,156	470,313	11 GiB, 105 MiB

*Table 2: Icosatree Building Statistics*

The barycentric coordinate based Icosatree subcells allowed for the point data construction to better fit the resulting data as the trees were better filled by the creation algorithm and created far fewer tree cells than the Octree or the axis-aligned Icosatree. However, because efficiently creating an index into a triangle wasn't directly apparent, a naive axis-aligned approach was used in the end. Unfortunately, partitioning the triangle by the u-v barycentric coordinates resulted in the points being skewed toward every other cell and attempting to use a ternary plot approach proved just as fruitless. A brute force partition of the tree could have been implemented but it would have required a large number of triangular prism bounding volumes be used for sub cell insertion which seemed excessively slow and was abandoned for the axis-aligned approach.

## Point Selection and Triangulation

The Point Selection and Triangulation is implemented with a number of options. First, the CAST algorithm used a Marching Cubes algorithm to compute point densities and prune all points above a certain threshold; this was implemented early on but the issues with using a structured point cloud like San Simeon, CA became apparent. The marching cubes approach ended up removing most of the points selected or almost none at all. In the end, the screen-space lasso was the only portion of the paper implemented. This created a projected frustum into the scene which was used to cull points outside of the selection.

Next, the screen-space point pruning was implemented in a few different ways. The application of which

is tunable as well as the run order of each portion implemented. The first pruning algorithm added was a naive altitude offset where the min/max altitude range of all points selected was computed and then the nth lowest percentage were removed. Second, an orthonormal threshold was added where, for each point, the k-nearest neighbors were queried. The orthonormal vector was found by computing the eigenvectors for the set of neighbors and if this vector was within a certain threshold of the global eigenvector normal, the point was discarded. Last, the screen-space operator pruning algorithm was used to remove any points that were obstructed by other points by using distance to the camera and an angle threshold between the vector from the tested point and all other points in the selection. If the tested point was behind another point and the angle between its camera vector and the other points' camera vector failed a threshold value, the point was discarded.

Once the point pruning is completed, all points are converted into x,y global eigenvector space and inserted into a map to preserve the local-to-world position pair. The local-space vertices were then sent through a Delaunay triangulation algorithm pass and all triangles exported are then converted back into world coordinates using the local-to-world coordinate mappings.

Below are a few more point selection and triangulation examples.



*Illustration 13: Point Selection with Lasso*

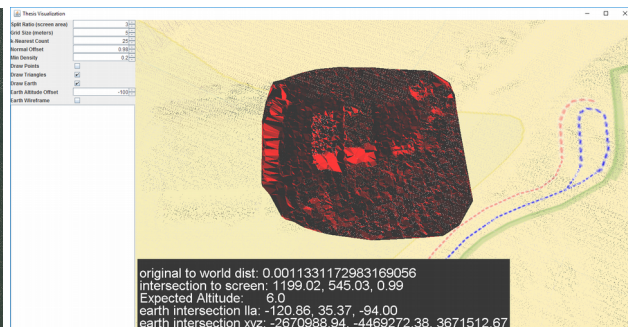


*Illustration 14: Selection Triangulation*



**Illustration 15: Selection Triangulation with Obstruction Pruning**

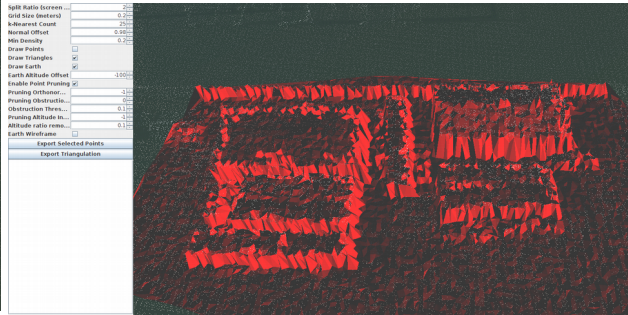


**Illustration 16: Selection Triangulation Closeup**

## Octree vs Icosatree Cell Size and Rendering Statistics

The Octree was initially chosen as the data structure for the point cloud data as it allowed a global dataset to be handled without the need to deal with geodetic coordinates and that the cartesian coordinate space parallels directly with the graphics pipeline. The axis-aligned nature of the cells also allows for efficient culling of the dataset during rendering. However, the Octree structure does not follow the projected surface of the Earth well and there is a large portion of the Octree structure that is never used. The Icosatree structure was chosen as a potential alternative because it aligns with the Earth's projected surface more closely, each cell in the tree splits into child cells whose volume can be filled more efficiently, and the handling of the tree file structure is identical to the Octree version so can be used as a direct replacement with very little additional modification and the tree can be traversed with little additional overhead. Also, because the tree cells are filled more efficiently, data usage in the vertex buffer should be less wasteful compared with the Octree implementation. Below, in Table 3 and Table 4, are tables of subcell sizes, including cartesian dimensions, surface area, and volume for cells at a number of select tree depths.

Tree Depth	Type	X-Span (m)	Y-Span (m)	Z-Span (m)	Side Area ( $m^2$ )	Volume ( $m^3$ )
18	AABB	64	64	64	4096	262144
19	AABB	32	32	32	1024	32768
20	AABB	16	16	16	256	4096
21	AABB	8	8	8	64	512
22	AABB	4	4	4	16	64

**Table 3: Octree Cell Statistics**

Tree Depth	Type	X-Span (m)	Y-Span (m)	Z-Span (m)	Depth (m)	Top Area (m^2)	Bottom Area (m^2)	Volume (m^3)
18	Triangle Prism	83.7769	95.9998	64.0	29.8935	2709.8502	2709.8296	81006.642
19	Triangle Prism	41.8885	48.0	32.0	14.9468	677.4626	677.46	10125.8496
20	Triangle Prism	20.9443	24.0	16.0	7.4734	169.3656	169.3653	1265.7324
21	Triangle Prism	10.4721	12.0	8.0	3.7367	42.3414	42.3414	158.2166
22	Triangle Prism	5.2361	6.0	4.0	1.8683	10.5854	10.5853	19.7771

*Table 4: Icosatree Cell Statistics*

As can be seen from the tables above, The dimensions and volumes of the two tree variations are comparable in absolute cartesian bounds but their internal volumes are much different. With the Icosatree cells being smaller but aligned with the projected surface of the dataset they are filled more efficiently as seen in Table 1 and Table 2. This allows the rendering system to display fewer cells in order to render the same amount of data while only adding a small amount of processing time when computing frustum culling per cell which, overall, is still comparable by per cell time (0.16 ms /cell vs. 0.19 ms/cell) as seen in Table 5. However, it also adds a bit of point overdraw where the cells that fill the frustum contain more points outside the viewable area but are still drawn as their parent cell intersects the frustum and contains some points within this area. Since the cell fits better with the dataset projection, points will tend to fill the larger, less deep, cells in the tree. The oriented axis cells perform better than the axis-aligned cells as seen by comparing the Octree performance and the Icosatree with axis-aligned cells compared to the Icosatree with oriented cells. The test performed below was on the 100x100x100 subcell datasets with the level-of-detail set to maximum; this requires a higher-than-normal per-frame time but was used to show the tree rendering between each type as close to comparable as possible. The camera was set at a specific location before starting the application so that each run was consistent. An example of the rendering result can be seen in Illustration 17.

Cell Type	Point Count	Cell Count	Culling	Rendering	Building Bounds
Icosatree (100x100)	3355393	1276	252 ms	1 ms 172 $\mu$ s	265 $\mu$ s
Icosatree (150x100)	6065591	1533	236 ms	1 ms 402 $\mu$ s	220 $\mu$ s
Icosatree (200x100)	7325988	1522	187 ms	1 ms 765 $\mu$ s	325 $\mu$ s
Octree (AABB)	3692901	630	103 ms	755 $\mu$ s	91 $\mu$ s

*Table 5: Rendering Statistics (depth = 10.0)*



*Illustration 17: Rendering Statistics Sample Image (depth = 10.0)*

If the depth ratio is reduced to a more reasonable use-case, the comparisons between using the Octree and Icosatree become less pronounced and more manageable as seen in Table 6 and Table 7. The number of points rendered is slightly higher in the Icosatree implementation than with the Octree, and per-frame times are increased as well. This is due in part to the smaller altitude component of the icosahedron cell handling less point data than the much more massive octree cells. As seen in table Table 3 and Table 4, the depth of the icosahedron cells limits the amount of data the cells can handle vertically along the projected surface when compared to the octree cells. In future implementations, this might be alleviated by not splitting every cell along its depth; such as all cells above a certain depth threshold or every third split, for example.

Cell Type	Point Count	Cell Count	Culling	Rendering	Building Bounds
Icosatree (100x100)	1097116	200	67 ms	636 $\mu$ s	53 $\mu$ s
Icosatree (150x100)	2280826	201	47 ms	408 $\mu$ s	60 $\mu$ s
Icosatree (200x100)	3825534	201	96 ms	332 $\mu$ s	52 $\mu$ s
Octree (AABB)	880582	99	39 ms	379 $\mu$ s	35 $\mu$ s

*Table 6: Rendering Statistics (screen ratio = 3.0)*

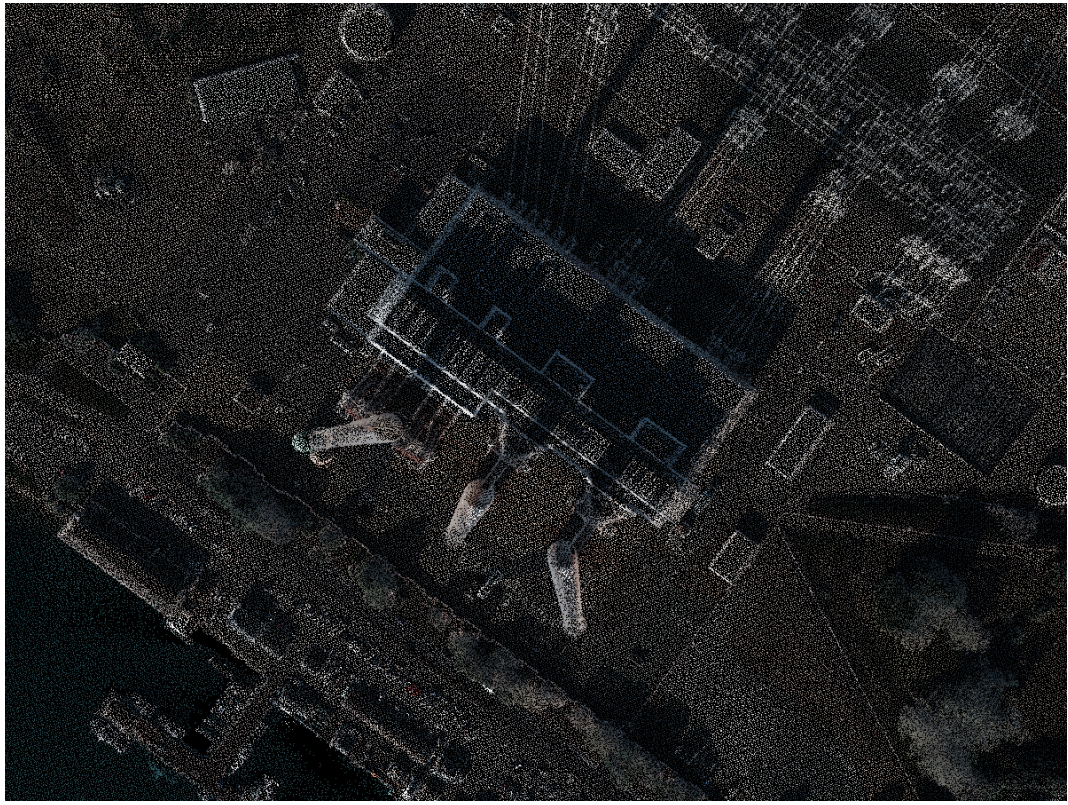


Illustration 18: Rendering Statistics Sample Image (depth = 3.0)

Cell Type	Point Count	Cell Count	Culling	Rendering	Building Bounds
Icosatree (100x100)	2391155	494	138 ms	910 $\mu$ s	310 $\mu$ s
Icosatree (150x100)	4368414	494	92 ms	630 $\mu$ s	140 $\mu$ s
Icosatree (200x100)	6239669	493	110 ms	502 $\mu$ s	87 $\mu$ s
Octree (AABB)	1915896	223	126 ms	312 $\mu$ s	46 $\mu$ s

Table 7: Rendering Statistics (screen ratio = 6.0)



*Illustration 19: Rendering Statistics Sample Image (depth = 6.0)*

## Chapter 6: Deliverables

Deliverables includes this final report detailing the outcome of the algorithms developed along with any source code developed when testing its validity. The report will also include examples and results data. Documentation for the source code will also be provided along with the source code itself.

## References

[1] Ruggero Pintus, Enrico Gobbetti, and Marco Agus. 2011. Real-time rendering of massive unstructured raw point clouds using screen-space operators. In Proceedings of the 12th International conference on Virtual Reality, Archaeology and Cultural Heritage (VAST'11), Matteo Dellepiane, Sebastian Pena Serna, Holly Rushmeier, Luc Van Gool, and Franco Niccolucci (Eds.). Eurographics Association, Aire-la-Ville, Switzerland, Switzerland, 105-112.

DOI=<http://dx.doi.org/10.2312/VAST/VAST11/105-112>

[2] Lingyun Yu, Konstantinos Efstathiou, Petra Isenberg, Tobias Isenberg. CAST: Effective and Efficient User Interaction for Context-Aware Selection in 3D Particle Clouds. IEEE Transactions on Visualization and Computer Graphics, Institute of Electrical and Electronics Engineers, 2016, 22 (1), pp.886-895.<10.1109/TVCG.2015.2467202>.

[3] Wenzel K, Rothermel M, Fritsch D, Haala N. An out-of-core Octree for massive point cloud processing. In: Workshop on processing large geospatial data Cardiff, UK, July 8th, 2014, {<http://rs.tudelft.nl/~rlindenbergh/workshop/WenzelIQmulus.pdf>}; 2014.

[4] Goswami, P.; Yanci Zhang; Pajarola, Renato; Gobbetti, E., "High Quality Interactive Rendering of Massive Point Models Using Multi-way kd-Trees," in Computer Graphics and Applications (PG), 2010 18th Pacific Conference on , vol., no., pp.93-100, 25-27 Sept. 2010 doi: 10.1109/PacificGraphics.2010.20

[5] Rico Richter and Jürgen Döllner. 2010. Out-of-core real-time visualization of massive 3D point clouds. In Proceedings of the 7th International Conference on Computer Graphics, Virtual Reality, Visualisation and Interaction in Africa (AFRIGRAPH '10). ACM, New York, NY, USA, 121-128.

DOI=<http://dx.doi.org/10.1145/1811158.1811178>

[6] Sriram Krishnan, Christopher Crosby, Viswanath Nandigam, Minh Phan, Charles Cowart, Chaitanya Baru, and Ramon Arrowsmith. 2011. OpenTopography: a services oriented architecture for

community access to LIDAR topography. In Proceedings of the 2nd International Conference on Computing for Geospatial Research & Applications (COM.Geo '11). ACM, New York, NY, USA, , Article 7 , 8 pages. DOI=<http://dx.doi.org/10.1145/1999320.1999327>

[7] Yingxin Wu, Masahiro Takatsuka, Spherical self-organizing map using efficient indexed geodesic data structure, Neural Networks, Volume 19, Issues 6–7, July–August 2006, Pages 900-910, ISSN 0893-6080, <http://dx.doi.org/10.1016/j.neunet.2006.05.021>.

[8] Michael Lee, Hanan Samet, Traversing the Triangle Elements of an Icosahedral Spherical Representation in Constant-Time, In Proc. 8th Intl. Symp. on Spatial Data Handling, Vancouver, Canada, July 1998, pp. 22–33

[9] Denis White, Global Grids from Recursive Diamond Subdivisions of the Surface of an Octahedron or Icosahedron, Environmental Monitoring and Assessment September 2000, Volume 64, Issue 1, pp 93-103

[10] By David Eppstein - self-made; originally for a talk at the 21st ACM Symp. on Computational Geometry, Pisa, June 2005, Public Domain, <https://commons.wikimedia.org/w/index.php?curid=2489019>

[11] By WhiteTimberwolf, PNG version: Nü - Own work, CC BY-SA 3.0, <https://commons.wikimedia.org/w/index.php?curid=9851485>

[12] By KiwiSunset at the English language Wikipedia, CC BY-SA 3.0, <https://commons.wikimedia.org/w/index.php?curid=16242249>

[13] By MYguel - Own work, Public Domain, <https://commons.wikimedia.org/w/index.php?curid=4535483>

[14] By User:DTR - Vectorisation of Image:Icosahedron.jpg, CC BY-SA 3.0, <https://commons.wikimedia.org/w/index.php?curid=2231553>

[15] "LiDAR and Raster Datasets Covering 1,500 Sq. Km. of the CA Central Coast Now Available." *LiDAR and Raster Datasets Covering 1,500 Sq. Km. of the CA Central Coast Now Available*. Pacific Gas & Electric Company (PG&E), n.d. Web. 26 Aug. 2016,  
<http://www.opentopography.org/news/lidar-and-raster-datasets-covering-1500-sq-km-ca-central-coast-now-available>